Available online at www.sciencedirect.com
SCIENCE DIRECT®
Chemical Physics 316 (2005) 178–184
Chemical Physics
www.elsevier.com/locate/chemphys

Internal rotation of methyl group in 2- and 1-methylanthracene studied by electronic spectroscopy and DFT calculations

Masayuki Nakagaki, Eriko Nishi, Kenji Sakota, Kaori Nishi [1], Haruyuki Nakano, Hiroshi Sekiya *

Department of Molecular Chemistry, Graduate School of Sciences, Kyushu University, 6-10-1 Hakozaki, Higashi-ku, Fukuoka 812-8581, Japan
Department of Chemistry, Faculty of Sciences, Kyushu University, 6-10-1 Hakozaki, Higashi-ku, Fukuoka 812-8581, Japan

Received 16 February 2005; accepted 6 June 2005
Available online 15 July 2005

Abstract

The S_1–S_0 fluorescence excitation and dispersed fluorescence spectra of 2- and 1-methylanthracene are measured in a supersonic free jet expansion. The barrier heights to internal rotation in the S_0 and S_1 states of 2-methylanthracene are determined to be 69 and 335 cm^{-1}, respectively, by using a one-dimensional free-rotor model. A prominent 0–0 transition has been observed in the fluorescence excitation spectrum of 1-methylanthracene, but no methyl rotational bands have been detected in both the excitation and dispersed fluorescence spectra. The potential energy curves of the methyl rotation are obtained for 2- and 1-methylanthracene with density functional theory (DFT) calculations and time-dependent (TD)-DFT calculations at the B3LYP/6-31 + G(d,p) level. The barrier heights and the phase of the potential energy curve are very different between 2- and 1-methylanthracene and substantially depend on the electronic state. These differences are consistently explained by a $\pi^*-\sigma^*$ hyperconjugation effect introduced by Nakai and Kawai [Chem. Phys. Lett. 307 (1999) 272].
© 2005 Elsevier B.V. All rights reserved.

Keywords: Methyl rotation; Methylanthracene; Electronic spectrum; Supersonic free jet; Density functional theory calculation; Fluorescence; Hyperconjugation

1. Introduction

The internal rotation of the methyl group in the S_0 and S_1 states and ground-state cation (D_0) of many aromatic molecules has been extensively studied by measuring the electronic spectra and pulsed-filed zero-kinetic energy (PFI-ZEKE) photoelectron spectra in a supersonic molecular beam [1–13]. These studies reveal that the internal rotational potential is very sensitive to the substituted position of the methyl group and the electronic state. The analysis of the internal rotational potentials has provided insight into non-covalent interaction and the intramolecular vibrational energy redistribution. It is crucial to determine the methyl rotational potentials to discuss the non-covalent interaction between the methyl group and the aromatic ring. The origin of the rotational barrier to internal rotation in the methyl-substituted aromatic molecules has been theoretically investigated. The barrier heights are correlated with the difference in the bond order of the C–C bond and with that in the charge [14,15]. Such a theory is useful for analyzing the methyl rotational potentials of the S_0 and D_0 states, but inapplicable to the change

* Corresponding author.
E-mail address: hsekiscc@mbox.nc.kyushu-u.ac.jp (H. Sekiya).
[1] Present address: 1-154-210, Morinosato, Kanazawa-shi, Kanazawa 920-1167, Japan.

0301-0104/$ - see front matter © 2005 Elsevier B.V. All rights reserved.
doi:10.1016/j.chemphys.2005.06.006

in the barrier upon $S_1 \leftarrow S_0$ excitation [16]. Nakai and coworkers [16–20] introduced a new model, which is based on a $\pi^*-\sigma^*$ hyperconjugation (HC) effect between the π^* orbital of the carbon atom and the σ^* orbital of the hydrogen atoms of the methyl group. This model has been successfully used to explain the stability of the lowest unoccupied molecular orbitals (LUMOs) and the highest occupied molecular orbitals (HOMOs) of several molecules such as substituted toluenes [17,19,20] and 1- and 2-methylnaphthalene [18].

In this work, we focus on the difference in the internal rotation of the methyl group in 2-methylanthracene (2MA) and 1-methylanthracene (1MA). The methyl rotation in 2MA was investigated by measuring the laser fluorescence excitation (LIF) spectrum [21]. The barrier to internal rotation was obtained for the S_1 state. However, the barrier for the S_0 state was predicted by calculating the Franck–Condon factors for the S_1–S_0 transition, while the rotational levels in the S_0 state were not determined. To our best of knowledge, there has been no report on the electronic spectrum of 1MA. In 1MA the distance between a hydrogen atom of the methyl group and the nearest CH hydrogen atom(s) is much shorter than that in 2MA. The steric repulsion may significantly influence the shape of the potential energy surface. The S_1–S_0 electronic spectra of the two molecules have been measured in a supersonic free jet expansion to investigate the effect of the non-covalent interaction on the methyl rotational potential energy surface. The stable geometries and potential energy curves of methyl rotation for the S_0 and S_1 states have been calculated with density functional theory (DFT) and time-dependent (TD)-DFT calculations, respectively. The shape of the internal rotational potential curve remarkably depends on the substituted position of the methyl group in the anthracene ring. The origin of the variations of the barrier heights and the phase of the potential upon electronic excitation has been discussed.

2. Experiment

2MA and 1MA were purchased from Wako Pure Chemical Ind. Ltd., and were used without further purification. The experimental apparatus for the measurement of the LIF and dispersed fluorescence (DF) spectra was essentially the same as that reported previously [22,23]. Briefly, 2MA or 1MA was vaporized by heating the solid sample in a nozzle housing to 100–120 °C. Gas mixture of the vaporized molecules and helium was expanded into a vacuum chamber with a pulsed nozzle (General Valve Series 9, 0.5 mm orifice diameter). The backing pressure was 200–300 kPa. An excimer laser pumped dye laser system (Lumonics EX-600 and HD-300) excited the molecules seeded in the helium gas. LIF spectra were measured by monitoring total fluorescence with a photomultiplier tube (Hamamatsu 1P28A). DF spectra were measured with a monochromator equipped with a photomultiplier tube (Hamamatsu R955). The electric current from the photomultiplier tubes was fed into a digital oscilloscope (LeCroy 9310A) and processed by a PC.

3. Results

3.1. LIF and DF spectra

Fig. 1(a) and (b) display the $S_1 \leftarrow S_0$ ($\pi\pi^*$) LIF spectra of 2MA and 1MA around the electronic origin region. The S_1–S_0 origin of 2MA is observed at 27389 cm^{-1}. Several methyl rotational bands are assigned in the figure. The procedure for assigning the rotational levels is described in Section 3.2. The LIF spectrum of 2MA is essentially the same as that reported previously [21]. A strong band is observed at 27463 cm^{-1} in the LIF spectrum of 1MA. This band

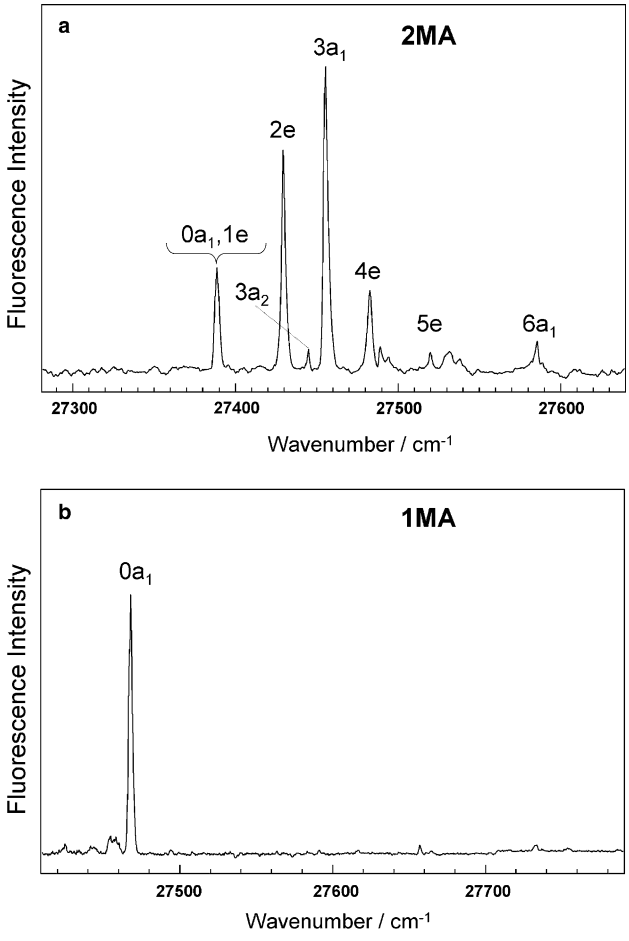

Fig. 1. LIF spectra of jet-cooled (a) 2MA and (b) 1MA. The assignments for the rotational levels of 2MA are indicated in the figure.

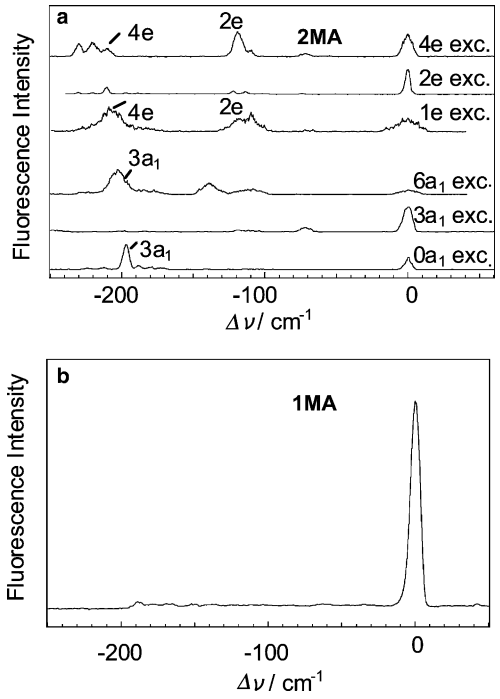

Fig. 2. DF spectra of jet-cooled (a) 2MA and (b) 1MA. The assignments for the rotational levels of 2MA are indicated in the figure.

has been assigned to the S_1–S_0 origin (0–0 or $0a_1$–$0a_1$) of 1MA. In the $\Delta\nu = 0$–300 cm^{-1} region no vibronic band is detected.

Fig. 2(a) and (b) display the DF spectra of 2MA and 1MA, obtained by exciting to various transitions. The DF spectrum of 2MA was not reported in the previous study [21]. Fig. 2(b) shows the DF spectrum of 1MA measured by exciting the origin band. No low-frequency bands are observed in the $\Delta\nu = 0$–250 cm^{-1} region in Fig. 2(b). The LIF and DF spectra of 1MA indicate that the transitions between the internal rotational levels are too weak to be observed. We will discuss the reason for the non-observation of the methyl rotational bands in the LIF and DF spectra of 1MA in Section 3.3.

3.2. Internal rotational potential curves for 2MA

The internal rotational energy levels in the S_0 and S_1 states of 2MA are analyzed using a V_3–V_6 potential in a one-dimensional rotor model [9,24]. The potential for internal rotation is expressed by

$$V(\theta) = \frac{1}{2}V_3(1-\cos 3\theta) + \frac{1}{2}V_6(1-\cos 6\theta), \quad (1)$$

where θ would be the torsional angle between the methyl group and molecular plane. The Schrödinger equation is given by

$$\left\{-B\frac{d^2}{d\theta^2} + V(\theta)\right\}\Psi_m(\theta) = E_m\Psi_m(\theta), \quad (2)$$

where B is the reduced internal rotational constant of the methyl rotor around the methyl top axis. A basis set of harmonic one dimensional free rotor wave functions $\cos(m\theta)$ and $\sin(m\theta)$ is employed to determine the eigenvalue of the Hamiltonian. For the calculation 50 basis functions ($m = 0$–5) are used for both even and odd symmetry. The assignments for the rotational levels in the S_1 state of 2MA are essentially the same as those reported previously [21], where a combination of the rotational quantum number m $(0, 1, 2, \ldots)$ of a one-dimensional free rotor with the symmetry species $\sigma(a_1, a_2, e)$ of a permutation-inversion-symmetry group G_6 isomorphous with C_{3v} are used to label the rotor level.

The observed and calculated internal rotational levels in the S_1 and S_0 states of 2MA are listed in Tables 1 and 2 together with the assignments. The observed and calculated internal rotational levels and the assignments for the S_1 states in this work are in good agreement with those reported by Lin et al. [21]. The rotational constant B is determined to be 5.2 cm^{-1} both for the S_0 and S_1 states of 2MA, and the V_3 barrier heights are 69 and 335 cm^{-1} for the S_0 and S_1 states, respectively. The V_6 barrier is 0 cm^{-1} for the S_0 and S_1 states. The phase of the internal rotational potential curve changes 60° upon S_1–S_0 excitation. A value $V_3 = 69$ cm^{-1} is in good agree-

Table 1
Observed and calculated rotational states in S_1 of 2MA

$\Delta\nu/cm^{-1}$				Assignment
Observed (This Work)	Calculated (This Work)[a]	Observed (Ref. [21])	Calculated (Ref. [21])[b]	
0.0	0.0	0.0	0.0	$0a_1$
2	1.6	2–3	1.7	1e
40	40.2	40	39.3	2e
56	55.5	56	55.5	$3a_2$
67	67.3	67	66.4	$3a_1$
94	96.2	95	96.3	4e
143	141.3	145	142.2	5e
199	197.2	198	199.0	$6a_1$

[a] Obtained with parameters $B = 5.12$ cm^{-1} and $V_3 = 73$ cm^{-1}.
[b] Obtained with parameters $B = 5.2$ cm^{-1} and $V_3 = 70$ cm^{-1} (Ref. [21]).

Table 2
Observed and calculated rotational states in S_0 of 2MA

$\Delta\nu/cm^{-1}$		Assignment
Observed	Calculated[a]	
0.0	0.0	$0a_1$
119	119.2	2e
197	197.2	$3a_1$
210	210.1	4e

[a] Obtained with parameters $B = 5.12\ cm^{-1}$, $V_3 = 292\ cm^{-1}$, and $V_6 = 35\ cm^{-1}$.

ment with the reported value ($70\ cm^{-1}$) [21]. We calculated the Franck–Condon factors for the S_1–S_0 transition to determine the phase change between the internal rotational potentials of the S_1 and S_0 states. The calculated intensities for the absorption and emission are compared in Fig. 3. The best fits are obtained when the phase of the internal rotational potential curve changes 60° upon S_1–S_0 excitation.

The internal rotational potential energy curves could not been determined for 1MA from the experimental data, because the intensity of the S_1–S_0 transition is concentrated on the origin and the transitions in the another rotational levels are two weak to be detected.

3.3. Theoretical internal rotational potential curves

Calculations were performed with a GAUSSIAN program package [25] for the S_0 and S_1 states, respectively. Optimization was first carried out for the S_0 state with DFT calculations at the B3LYP/6-31 + G(d,p) level. In 1MA and 2MA, the stable conformations obtained from first optimization were defined as the rotational angle $\theta = 0^\circ$, where one of the C–H bonds of the methyl group is in the plane of the anthracene ring and one of the CH bonds of the methyl group eclipses the C–C bond in the anthracene ring as drawn in Fig. 4. Geometry optimization was performed at each rotational angle to obtain the energy curves for the methyl rotation. The rotational angle was varied from 0° to 120° at 10° intervals. Single point energy calculations were carried out for the S_1 state of the three molecules by TD-DFT calculations at the B3LYP/6-31 + G(d,p) level, where the optimized structures for the S_0 state are used.

Fig. 5 shows the rotational potential energy curves for the S_0 and S_1 state of 2MA and 1MA, as a function of the rotational angle (θ) together with the orbital energies. The calculated phase change is consistent with the experimental result. The calculated potential barrier

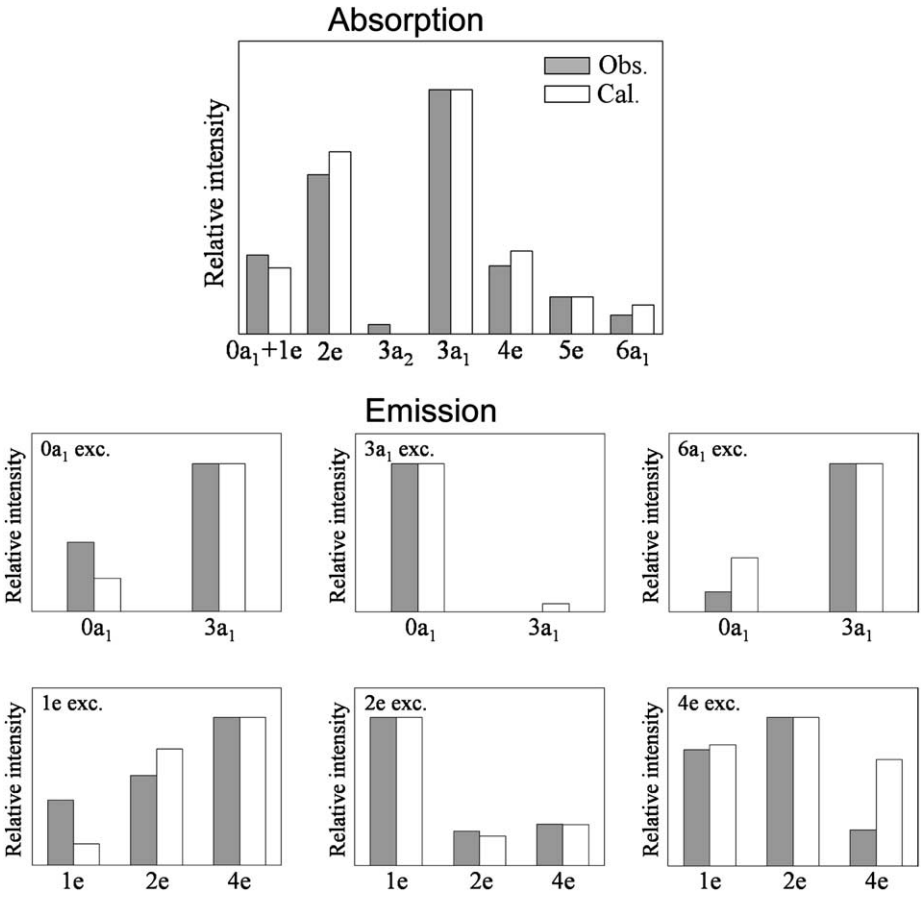

Fig. 3. Comparison of the observed and calculated intensities for the S_1–S_0 absorption and emission between the internal rotational states. The observed and calculated intensities are drawn with the shaded and white bars, respectively.

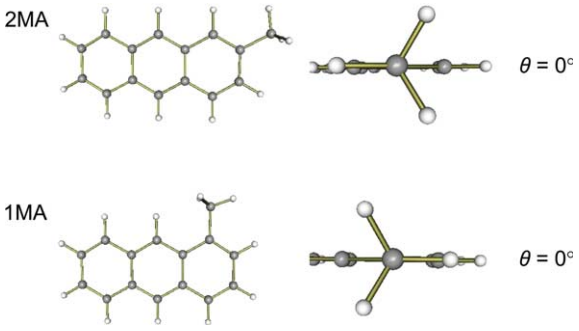

Fig. 4. Top and side views are drawn for the optimized conformations of the methyl group in the S_0 states of 2MA and 1MA.

heights to internal rotation of the methyl group in 2MA and 1MA are summarized in Table 3. The V_3 barriers for the S_0 and S_1 states are calculated to be 302 and $-215\ cm^{-1}$, respectively. The V_3 barrier of $302\ cm^{-1}$ for the S_0 state is in agreement with the experimental value of $335\ cm^{-1}$. The calculated V_3 barrier of $-215\ cm^{-1}$ is larger than the experimental value of $69\ cm^{-1}$, however the calculated V_3 barriers are qualitatively in agreement with the relation $|V_3(S_0) > |V_3(S_1)|$ obtained from experiment.

The potential energy curves for 1MA indicate that no phase shift occurs upon S_1–S_0 excitation. Therefore, the intensity of the transition must be concentrated on the 0–0 transition. The observation of the prominent 0–0 transition is consistent with the calculated potential energy curves. The calculated V_3 barrier heights for the S_0 and S_1 states are 790 and $477\ cm^{-1}$, respectively. These barrier heights are substantially higher than the corresponding ones for 2MA.

Table 3
Calculated potential barrier heights to internal rotation of the methyl group in methylanthracenes in units of cm^{-1}[a]

Molecule	S_0		S_1	
	V_3	V_6	V_3	V_6
2MA	302 ± 1	-10 ± 1	-215 ± 1	-7 ± 1
1MA	790 ± 4	-13 ± 4	477 ± 5	-6 ± 5

[a] The errors are obtained by the least squares fitting as the standard deviation.

4. Discussion

We have observed the LIF and DF spectra of 2MA and 1MA. We obtained the experimental potential energy curves of the methyl rotation in the S_0 and S_1 states for 2MA. No methyl rotational bands have been observed in the LIF and DF spectra of 1MA. This result is consistent with the theoretical potential energy curves of the methyl rotation for the S_0 and S_1 states, where no phase shift is seen between the two potential energy curves.

The appearance of the potential energy barrier to internal rotation in the aromatic molecules such as substituted toluenes and methylnaphthalenes has been consistently explained by the $\pi^*-\sigma^*$ HC effect [16–20]. According to Nakai and Kawamura, the $\pi^*-\sigma^*$ HC ap-

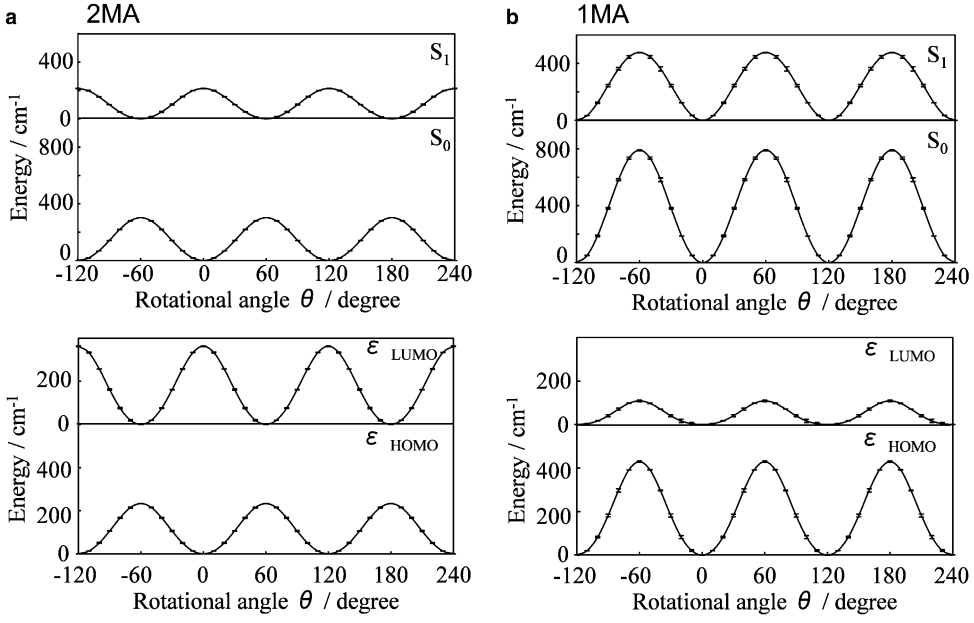

Fig. 5. Calculated potential energy curves for the S_0 and S_1 states (upper figures) and orbital energies (lower figures) of (a) 2MA and (b) 1MA. Solid lines are the fitting curves obtained by the least square method. The error-bars show the deviation of the DFT calculations from fitting curve.

pears between an unoccupied π* orbital of the benzene ring and an unoccupied C–Hσ* orbital in the LUMO. A similar HC effect occurs between an occupied π orbital and an unoccupied σ* orbital of the C–H bond in the HOMO. This effect is named π−σ* HC [18]. These two HC effects are different from the conventional HC effect, in which the HC appears between an occupied π orbital of the benzene ring and an occupied σ orbital of the C–H bond of the methyl group. For example, in 1-methylnaphathalene the π*−σ* HC causes a slightly bonding interaction between *ortho carbon atom* and *out-of-plane hydrogen atoms* of the methyl group and dominates the barrier change by the S_1–S_0 excitation [18].

We have examined the occurrence of the π*−σ* HC or π*−σ* HC effect in the three methylanthracenes by calculating the HOMOs and LUMOs. The orbital energy curves of the HOMO and LUMO for the two methylanthracenes are illustrated in Fig. 5. Fig. 6(a) and (b) show the energy variations ΔE in the $S_1 \leftarrow S_0$ excitation and the difference in the orbital energy ($\varepsilon_{LUMO} - \varepsilon_{HOMO}$) for the two anthracenes as a function of the rotational angle. The energy variations of the LUMO and HOMO for 2MA and 1MA, correlate well with those of ΔE. This means that the HOMO and/or LUMO contain the main factor for variations of the rotational energy barriers upon $S_1 \leftarrow S_0$ excitation, as is the case for 1- and 2-methylnaphthalene [18].

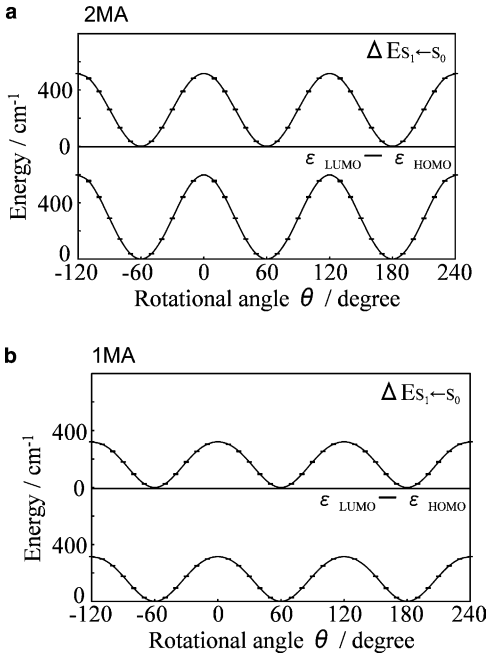

Fig. 6. Energy variations ΔE in the $S_1 \leftarrow S_0$ excitation and the difference in the orbital energy $\varepsilon_{LUMO} - \varepsilon_{HOMO}$ for (a) 2MA and (b) 1MA as a function of the rotational angle θ. Solid lines are the fitting curves obtained by the least square method. The error-bars show the deviation of the DFT calculations from fitting curve.

In 2MA, the V_3 barriers in the S_0 and S_1 states are in good agreement with the variations of the energies of the HOMO and LUMO. However, the calculated energies for the S_0 and S_1 states of 1MA are considerably larger than those for the HOMO and LUMO. This may be due to an additional contribution of a steric repulsion of the methyl group and the C–H_3 hydrogen (Fig. 4).

We have examined the π*−σ* HC effect on the shape of the internal rotational potential energy curves of the two methylanthracenes. Fig. 7(a) and (b) display the HOMOs and LUMOs of 2MA and 1MA. The sign of the coefficient of the wave functions of the σ* MO of the C–H bond of the methyl group and that of the π*MO or πMO in the anthracene ring is important. In 2MA, the π−σ* HC may occur at $\theta = 0^\circ$ in the HOMO, while π*−σ* HC may appear at $\theta = 60°$ in the LUMO. Thus, the energy of the HOMO and LUMO should be stabilized at $\theta = 0^\circ$ and $\theta = 60^\circ$, respectively.

The HOMOs and LUMOs of 1MA in Fig. 7(b) show that the π−σ* and π*−σ* HC may occur at $\theta = 0^\circ$ in the HOMO and LUMO, respectively, and the potential energy may stabilize at $\theta = 0^\circ$ in the both orbitals. The

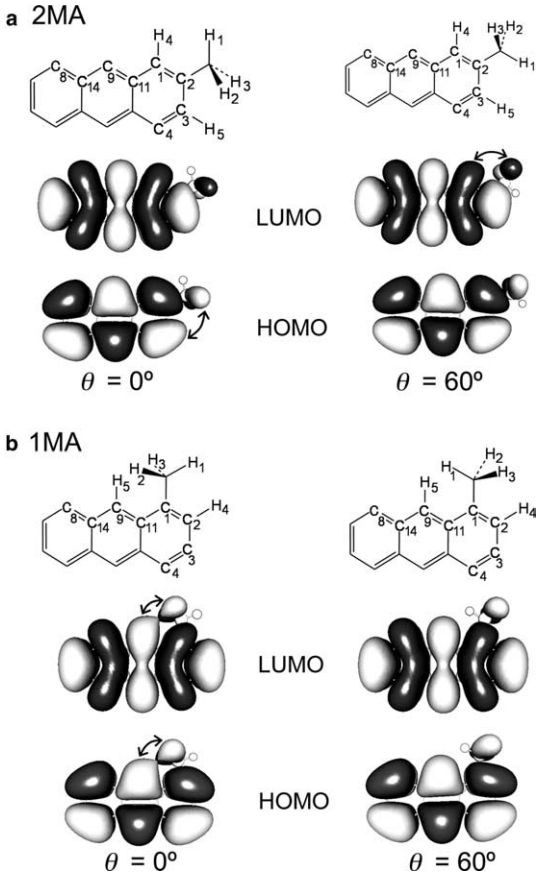

Fig. 7. Highest occupied molecular orbital (HOMO) and lowest unoccupied orbital (LUMA) of (a) 2MA and (b) 1MA at $\theta = 0^\circ$ and $\theta = 60^\circ$. The dark vs. light shading corresponding to different sign of the wave functions. The arrows indicate the occurrence of the π–σ* or π*–σ* HC effect.

signs of C–H_3 σ*MO and C_2–C_3 π*MO are the same at $\theta = 60^\circ$ in the LUMO, however an efficient π*–σ* HC effect will not occur since the overlapping of the π*MO and σ*MO is expected to be small.

5. Conclusions

The internal rotation of the methyl group in 2MA and 1MA has been investigated with electronic spectroscopy in the gas phase and theoretical calculations. The methyl rotational potential curves for the S_0 and S_1 states of 2MA are determined from the experimental spectra.

The observation of the strong S_1–S_0 origin and the absence of internal rotational bands in the LIF and DF spectra of 1MA are in agreement with the calculated potential energy curves of the methyl rotation for the S_0 and S_1 states, where no phase shift occurs upon $S_1 \leftarrow S_0$ excitation. The shape of the calculated potential energy curves in the S_0 and S_1 states of 2MA and 1MA are in agreement with those of the HOMO and LUMO of the corresponding molecule. The phase of the S_0 and S_1 potential energy curves of 2MA and 1MA are consistently explained by considering the π*−σ* or π−σ* HC effect, while the contribution of the steric repulsion is insignificant to determine the internal rotational potential of 1MA.

Acknowledgements

The authors wish to thank Prof. H. Nakai and Mr. M. Kawai (Waseda University) for valuable discussion. This work was supported in part by the Grant-in-Aid for Scientific Research No. 15250015 from the Japanese Ministry of Education, Science, Sports and Culture.

References

[1] K. Okuyama, N. Mikami, M. Ito, J. Phys. Chem. 89 (1985) 5617.
[2] H. Mizuno, K. Okuyama, T. Ebata, M. Ito, J. Phys. Chem. 91 (1987) 5589.
[3] T. Aota, T. Ebata, M. Ito, J. Phys. Chem. 93 (1989) 3519.
[4] X.-Q. Tan, W.A. Majewski, D.F. Plusquellic, D.W. Platt, J. Chem. Phys. 94 (1991) 7721.
[5] Z.Q. Zhao, C.S. Parmenter, D.B. Moss, A.J. Braley, A.E.W. Knight, K.G. Owens, J. Chem. Phys. 96 (1992) 6362.
[6] K.-T. Lu, G.C. Eiden, J.C. Weissharr, J. Phys. Chem. 96 (1992) 9742.
[7] K. Takazawa, M. Fujii, M. Ito, J. Chem. Phys. 99 (1993) 3205.
[8] M. Fujii, M. Yamauchi, K. Takazawa, M. Ito, Spectrochim. Acta 50A (1994) 1421.
[9] B. Ballesteros, L. Santos, Spectrochim. Acta Part A 58 (2002) 1069.
[10] K. Suzuki, S. Ishiuchi, M. Fujii, Faraday Discuss. 115 (2000) 229.
[11] K. Yoshida, K. Suzuki, S. Ishiuchi, M. Sakai, C.E.H. Dessent, K. Muller-Dethlefs, Phys. Chem. Chem. Phys. 4 (2002) 2534.
[12] S. Kinoshita, H. Kojima, T. Suzuki, T. Ichimura, K. Yoshida, M. Sakai, M. Fujii, Phys. Chem. Chem. Phys. 3 (2001) 4889.
[13] S. Ullrich, K. Muller-Dethlefs, J. Phys. Chem. A 106 (2002) 9181.
[14] Y. Sonoda, S. Iwata, Chem. Phys. Lett. 243 (1995) 176.
[15] K.-T. Lu, F. Weinhold, J. Weisshaar, J. Chem. Phys. 102 (1995) 6787.
[16] H. Nakai, M. Kawai, Chem. Phys. Lett. 307 (1999) 272.
[17] H. Nakai, M. Kawai, J. Chem. Phys. 113 (2000) 2168.
[18] H. Nakai, Y. Kawamura, Chem. Phys. Lett. 318 (2000) 298.
[19] M. Kawai, H. Nakai, Chem. Phys. 273 (2001) 191.
[20] Y. Kawamura, H. Nakai, Chem. Phys. Lett. 368 (2003) 673.
[21] H. Lin, J.A. Hunter, J. Pfab, Chem. Phys. Lett. 210 (1993) 38.
[22] H. Mori, H. Kugisaki, Y. Inokuchi, N. Nishi, E. Miyoshi, K. Sakota, K. Ohashi, H. Sekiya, J. Phys. Chem. A 106 (2002) 4886.
[23] N. Tanaka, C. Okabe, K. Sakota, T. Fukaminato, T. Kawai, M. Irie, A. Goldberg, S. Nakamura, H. Sekiya, J. Mol. Struct. 616 (2002) 113.
[24] C.C. Lin, J.D. Swalen, Rev. Mod. Phys. 31 (1959) 841.
[25] M.J. Frisch, G.W. Trucks, H.B. Schlegel, G.E. Scuseria, M.A. Robb, J.R. Cheeseman, J.A. Montgomery Jr., T. Vreven, K.N. Kudin, J.C. Burant, J.M. Millam, S.S. Iyengar, J. Tomasi, V. Barone, B. Mennucci, M. Cossi, G. Scalmani, N. Rega, G.A. Petersson, H. Nakatsuji, M. Hada, M. Ehara, K. Toyota, R. Fukuda, J. Hasegawa, M. Ishida, T. Nakajima, Y. Honda, O. Kitao, H. Nakai, M. Klene, X. Li, J.E. Knox, H.P. Hratchian, J.B. Cross, C. Adamo, J. Jaramillo, R. Gomperts, R.E. Stratmann, O. Yazyev, A.J. Austin, R. Cammi, C. Pomelli, J.W. Ochterski, P.Y. Ayala, K. Morokuma, G.A. Voth, P. Salvador, J.J. Dannenberg, V.G. Zakrzewski, S. Dapprich, A.D. Daniels, M.S. Strain, O. Farkas, D.K. Malick, A.D. Rabuck, K. Raghavachari, J.B. Foresman, J.V. Ortiz, Q. Cui, A.G. Baboul, S. Clifford, J. Cioslowski, B.B. Stefanov, G. Liu, Liashenko, P. Piskorz, I. Komaromi, R.L. Martin, D.J. Fox, T. Keith, M.A. Al-Laham, C.Y. Peng, A. Nanayakkara, M. Challacombe, P.M.W. Gill, B. Johnson, W. Chen, M.W. Wong, C. Gonzalez, J.A. Pople, GAUSSIAN 03, Revision A.2, Gaussian, Inc., Pittsburgh, PA, 2003.